Check for updates

Proceedings of the ASME 2026 45th International Conference on Ocean, Offshore and Arctic Engineering
OMAE2026
June 7-12, 2026, Tokyo, Japan

OMAE2026-177755

Downloaded from asmedigitalcollection.asme.org/OMAE/proceedings-pdf/OMAE2026/89480/V02AT02A050/7643410/v02at02a050-omae2026-177755.pdf by Deutsches Zentrum für Luft- und Raumfahrt (DLR) user on 22 October 2026

TEST STAND TO CONDUCT ACCELERATED AGEING AND DEGRADATION TESTS WITH STRUCTURAL MONITORING SENSORS

Eike Hohmann **Moritz Braun** **Sören Ehlers**

DLR – Institute of Maritime Technologies and Propulsion Systems
Geesthacht, Germany

ABSTRACT

In this study we present a test stand and procedure, to conduct experimental research on the degradation of sensors under accelerated ageing conditions, as induced by a maritime atmosphere. The test stand combines a vibrating beam structure and a corrosion test chamber. The beam functions as a carrier for the structural health monitoring (SHM) sensors under test. In the experiments, sensors like strain gauges, piezo electric acceleration sensors or temperature sensors can be mounted on the beam, inside the chamber. The suggested test program consists of baseline phases, in which the unaged sensors are characterized under stationary conditions, followed by accelerated ageing test cycles, incorporating alternating climates and salt fog. After each accelerated ageing cycle, the same baseline phases are repeated. The data analysis approach is a baseline comparison grounded on statistical features in the time- and frequency domain. Shifts in the features from one baseline cycle to another will be observed to determine decreases in data quality as a result of sensor ageing. The procedure is exemplified with two one-hour time series of a strain gauge. The research is expected to shed light on the reliability of SHM sensors under maritime environmental conditions and help to generate hypotheses for further research. It is planned to enhance the test stand and improve its control quality, to meet the requirements for certification tests in the future.

Keywords: Sensor ageing; structural health monitoring; corrosion test chamber; strain gauge; time series analysis

1. INTRODUCTION

SHM of marine structures allows early detection of structural damage or degradation and supports condition-based maintenance routines. Introduction of SHM systems also enables design optimization based on information about in service behavior [1]. Monitoring is achieved through monitoring systems, mainly consisting of sensor technology and data processing techniques. Thereby, strain-based approaches are among the most common ones for structure health monitoring, because strain measurements allow inference on structural stresses and deformations. Electrical strain gauge sensors are widely used in these approaches, due to their relatively low production costs and extensive experience with their industrial and scientific application. In the domain of ship structure and condition monitoring, they have been applied to measure hull girder longitudinal stresses, local ice loads or shaft-line operational loads [2-4]. Meanwhile, fiber Bragg grating sensors are also increasingly considered in ship SHM to measure hull deformations or monitor local hull features [5]. In full-scale measurement campaigns, strain measurements are often combined with accelerometer measurements, to capture the whole ship response in terms of rigid body motions, accelerations and strains [6]. Acceleration sensors also play a vital role in condition monitoring of heavy machinery. Piezoelectric accelerometers, for instance, are commonly used in monitoring of bearings, gear boxes, electric motors or other rotating machinery [7].

Regarding the processing of sensor data, in recent years, machine learning and deep learning models as well as digital twins have received increasing attention. In the latter, sensor data is used to update the digital representation of a physical object, more or less in real time. For example, Wei et al. introduce a digital twin methodology for the real-time monitoring of ship structure deformation fields [8]. In sensor networks, data fusion has become a common approach to generate more consistent and more dependable estimates of the whole system, using probabilistic, statistical, knowledge-based, inference and reasoning methods [9].

The use of sensors naturally comes with uncertainties,

Copyright © 2026 by ASME; reuse license CC-BY 4.0

affecting the accuracy and reliability of a measurement due to sensor characteristics, operational conditions and human or procedural factors. Meanwhile, the use of sensors to assess large marine structures comes with its own challenges. Local measurements need to be combined with simulation models, to make statements about global structure behavior or to derive the desired output quantities. For example, Böhm et al. discuss that for common instrumentation, ice loads can only be accurately determined, if the ice load acts within the instrumented area [3]. In the field of the instrumentation of marine structures, often a small number of sensors is required to obtain information about a great number of modes. Hence, the optimal positioning of sensors is an important topic in this domain [1].

Sensor data is regularly used to measure material and structure behavior. It is recognized that operation over time leads to some kind of ageing or degradation of a structure. Meanwhile, the ageing of the monitoring system itself is rarely considered. Bartels et al. underline, “these systems are often assumed to exhibit linear time-invariant behavior, although over time, their performance is affected by environmental factors and internal degradation, resulting in time-variant behavior” [10]. In the case of marine structures, it is particularly important to consider the impact of the harsh environmental conditions, on the measuring equipment. In its class guideline 0339, the classification society DNV defines environmental test specifications for electrical, electronic and programmable equipment and systems [11]. It provides a good overview about the relevant environmental parameters and ranges to be considered. Test programs and conditions depend on the intended installation location class on board but generally include increased humidity, alternating temperature profiles, vibrations and salty atmospheres. However, the aim of the guideline rather is to assure certain minimum standards for equipment durability, and not to investigate its ageing or degradation behavior.

We find, at least in in the domain of SHM of marine structures, sensor ageing did not get much attention in the past. We suggest to carry out more experimental research on the topic, with a focus on its impact on the quality of the acquired data. A sensor might operate reliably and within its expected margins of error for a certain time but the accuracy and other quality metrics might start to decrease at some point. The ultimate failure of a sensor is easy to detect, but the evaluation, if a signal acquired from a sensor is still reliable presupposes more knowledge about its ageing behavior. In the literature, specific failure modes and the behavior of specific sensors and devices have been addressed. Regarding strain gauges, dos Reis et al. describe two new methods for detecting strain gauge debonding faults and Khaled et al. investigate the influence of humidity on the zero signal of an amplifier for strain gauge measurements under application of a climatic chamber [12-13]. Bartels et al. investigate the performance of strain gauges in a static three-point bending testbed setting, within a climatic chamber, which is used to create temperature and humidity cycles to initiate aging processes [14]. The latter in deed confirmed that ageing effects lead to measurement drift and physical gain shifts, causing significant changes in the measurement signal. Different to the previously mentioned setup, our subsequently presented test stand is designed to allow a dynamic excitation of the sensors under test, besides the creation of humid and salty atmospheres, as those were identified as the main corrosive and destructive qualities of a maritime environment.

2. TEST STAND DESCRIPTION

The test stand consists of four main components: Beam structure, modal shaker system, corrosion test chamber, data acquisition system. The beam is manufactured from mild steel and was powder coated. It has a rectangular hollow section and a length of 2 m from support to support. One end features a pinned support while the other end has a sliding support. The modal shaker system consists of a signal generator, which provides a sine wave signal of the desired frequency, a power amplifier and the modal shaker. The latter translates the signal into up and down movement of a stinger, setting the beam into vibration with the specified frequency.



FIGURE 1: CORROSION TEST CHAMBER AND BEAM STRUCTURE

The beam can be excited with any desired frequency but due to size and weight of the beam, it only gives a considerable response when excited near its first Eigenfrequency at 42.2 Hz. Between beam and stinger, a force sensor is installed, measuring the excitation force. With the maximum allowed excitation of 100 N, at a frequency of 42.2 Hz, the peak-to-peak displacement in the center of the beam equals 2.8 mm with an acceleration amplitude of about 10 g. The beam thus represents a structure with a low-mid frequency vibrational behavior, which is within the typical range of a machinery area.

Downloaded from asmedigitalcollection.asme.org/OMAE/proceedings-pdf/OMAE2026/89480/V02AT02A050/7643410/v02at02a050-omae2026-177755.pdf by Deutsches Zentrum für Luft- und Raumfahrt (DLR) user on 22 October 2026

Copyright © 2026 by ASME; reuse license CC-BY 4.0

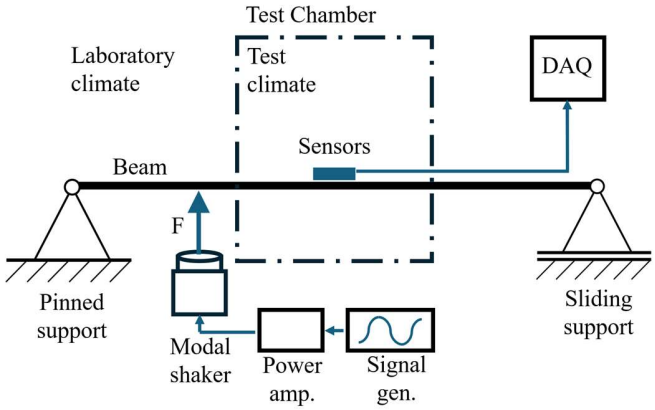


FIGURE 2: SKETCH OF THE IDEALIZED TEST SETUP

The stainless-steel corrosion test chamber has a capacity of 430 l and features a water outlet on the chamber's floor, a heating coil below the floor, a spray nozzle, a ventilation unit and a drainage outlet. The control system has a 10″ touch display and allows to program phases and chains of phases to form a test cycle. With the described features, it allows to increase the temperature inside up to 60 °C and create ∼95 % relative humidity, with water either being released onto the floor or sprayed into the center of the chamber through a nozzle. The chamber can be purged with ambient air, decreasing the temperature and humidity to ambient (laboratory) climate again. The water reservoir has a capacity of 140 l and is filled with desalinated water. Salt can be added to the water reservoir manually if required, to carry out tests with a NaCl-solution of up to 5 %. Between room climate and 60 °C, the temperature can be set in steps of 0.1 °C with a stability of ±1 °C. The chamber does not feature climatization, thus neither active cooling, besides purging the chamber with ambient air, nor specific air humidities between ∼95 % and laboratory conditions are feasible, as per now. Possible future expansions of the test stand limits are discussed in section 7. The chamber fulfills the requirements of several industrial corrosion test norms including ASTM B117 (salt spray test), ISO 11997-1 (cyclic salt spray test), ISO 6270 AT (condensing water test with alternating temperature phases) and others.

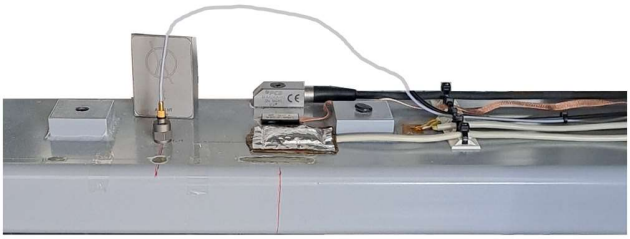


FIGURE 3: SENSORS MOUNTED ON THE BEAM INSIDE THE CHAMBER

[1] This only represents the accuracy of the data acquisition unit. The combined accuracy of a measurement can be much lower.

The beam passes through the corrosion test chamber and acts as the carrier for the sensors under test. The setup allows to mount sensors or devices on the beam, inside the chamber and thus expose them to the atmosphere and to the vibration of the beam.

The data acquisition system consists of a Gantner Q-station XT, together with several input modules covering strain gauges, as well as general analogue sensors and piezo electric (IEPE) sensors. The modules allow high accuracy up to ±0.1 % [1] and very high digitization rates of up to 100 kHz. The acquisition unit is connected to a server via Ethernet, where the time series data is stored.

TABLE 1: TEST STAND OPERATIONAL LIMITS

	Parameter	Min.	Max.	
Climate	Temperature	Lab. Temp.	60 °C	±1°C
	Rel. Humidity	Lab. Hum.	~95 %	
	Precipitation	0.5 l/h	3.0 l/h	±5 %
	Salt content	0.0 %	5.0 %	
Vibration	Eigenfrequency	42.2 Hz	-	
	Excitation	0 N	±100 N	±5 %
	Acceleration	0 g	±10 g	±5 %
	Amplitude	0 mm	±1.4 mm	±5 %
	Surface Strain	0 µm/m	±90 µm/m	±5 %

3. AGEING IDENTIFICATION

Sensor ageing and degradation are versatile and complex procedures. There is no unified theory to describe them. Ageing is a sum of different physical damage mechanisms, like corrosion, fatigue, moisture absorption, electrolytic effects, and others. The prevalent damage mechanisms of a sensor are highly dependent on the involved materials, fields and loads. Each damage mechanism describes a time-dependent change in certain material or structural parameters. But even though numerous physical effects can be involved, these alterations lead to a small set of fundamental observable anomalies in the sensor signal. Signal offset, drift, noise, shifts, spikes and data loss are the most typical anomalies, that apply to various sensor types. These anomalies can all be expressed by means of statistical properties, that can be derived from the time series data.

If a measurement is repeated with the same sensor under the same stationary conditions, the statistical properties of its time series data are expected to remain constant and stable.

As a sensor is ageing, even if a measurement is repeated under the same stationary conditions, we expect that shifts will be observable in certain statistical features of its time series data. Thus, the ageing of a sensor could generally be described as an advancing violation of the initial stability of its characteristic statistical properties.

Downloaded from asmedigitalcollection.asme.org/OMAE/proceedings-pdf/OMAE2026/89480/V02AT02A050/7643410/v02at02a050-omae2026-177755.pdf by Deutsches Zentrum für Luft- und Raumfahrt (DLR) user on 22 October 2026

Copyright © 2026 by ASME; reuse license CC-BY 4.0

4. TEST PROGRAM AND DATA ACQUISITION

We suggest to begin the test program with a baseline cycle, consisting of four phases with a duration of 1 h each. In addition, an initial 24 h baseline could be adequate. The duration of 24 h enables to detect and quantify the possible influence of daily proceedings in the laboratory and the day-night-cycle on the test stand and eventually the sensor signals. This is meant to avoid false interpretation of anomalies in the time series data later on. Certainly, the baseline comparison can also be executed based on shorter samples, as long as it is assured that the samples are gained under comparable conditions and are not influenced by unintended external disturbances. In each baseline phase one ambient parameter is altered, yielding four characteristic conditions: Standard, warm, wet and vibration (see table 2). The atmosphere is kept stationary during each phase. Depending on the design of the sensors under test, it should be considered that wet, warm and vibration conditions already pose a deviation from standard conditions, potentially initiating the degradation of the sensors. However, since this research happens in the context of SHM of marine structures, we assume the sensors under test tolerate these mild conditions at least in the short term. Strain gauges for instance will be covered with a protective putty and foil, following industrial best practice. Hence, the conditions are expected to be well suited to record baseline time series and allow to characterize the sensors' responses to different climates and mechanical conditions.

TABLE 2: SUGGESTED BASELINE TEST CYCLE

#	Dur.	Descript.	Properties		
			Temp.	Rel. Hum.[2]	Vibr.[3]
1	1 h	Standard	23±1°C	~50 %	-
2	1 h	Warm	40±1°C	~15 %	-
3	1 h	Vibration	23±1°C	~50 %	±2.5 g
4	1 h	Wet	23±1°C	~95 %	-

After the baseline cycle the first accelerated ageing cycle can be executed. The program suggested here is based on a cyclic corrosion test with three different climate phases within 24 h, in the style of the VW PV1210 standard. A salt fog phase is followed by a drying phase and warm condensing water phase. With respect to corrosiveness, the latter is among the strongest possible tests with the available chamber. [4] In addition to the corrosive atmospheres, the beam is set in vibration with maximum possible excitation during the drying phase of each 24 h cycle, to add a substantial mechanical load to the program. The duration of 24 h per cycle is typical in many industrial corrosion test norms and is adapted here for its good integrability into day-by-day laboratory working routines. Durations and conditions will be reconsidered depending on the first results.

[2] Relative humidity is determined by the humidity in the laboratory. Values for baseline phases 1-3 and accelerated ageing phase 2 are estimated average values.
[3] Intensity given as maximum acceleration of the beam surface.

TABLE 3: SUGGESTED ACCELERATED AGEING TEST CYCLE

#	Dur.	Properties		
		Temp.	Rel. Hum. [3]	Vibr. [4]
1	4 h	35±1 °C	salt spray [5]	-
2	4 h	25±1 °C	~50 %	±10 g
3	16 h	50±1 °C	~95 %	-
	↻	Repeated as necessary		

The sensor signals are digitized without any filtering and the data is continuously logged with a frequency of 1000 Hz. This digitization rate allows to analyze the dynamic responses of the sensors to the vibration of the beam with a decent resolution. For an excitation frequency of 42.2 Hz the resolution equals about 23 data points per oscillation. Even for the analysis of the signals of the static baseline phases, a high digitization rate grants high analytic depths in the frequency domain. However, down-sampling can be applied subsequently for certain steps of the statistical analysis, to handle computationally expensive steps in adequate time.

5. DATA ANALYSIS

For the data analysis, we suggest a baseline comparison, grounded on statistical properties in the time and frequency domain, acquired at different points in time. Other approaches, like, for instance, the installation of more accurate reference sensors and a successive deviation analysis do not seem practical in the present setup.

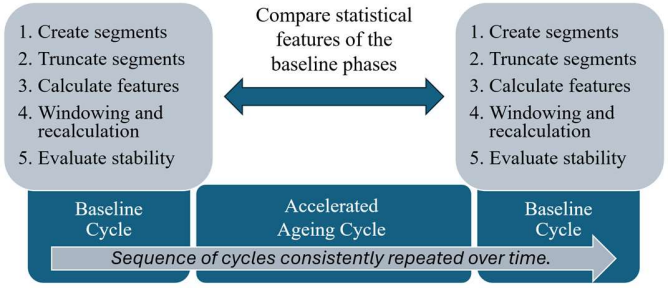


FIGURE 4: BASELINE COMPARISON SCHEME

As outlined in section 3, we assume that ageing is detectable through shifts in certain statistical properties of the time series. Hence, the derived features from the baseline phases before the accelerated ageing cycle are compared with the features from the baseline phases after the accelerated ageing cycle. Following general procedure is applied:

1. Divide the time series data into segments, covering one whole baseline phase each.

[4] Acetic acid tests are possible too but not considered for the time being.
[5] With 5% NaCl-solution (pH 6,5–7,2), Precipitation rate 1,0-2,0 ml/h per 80 cm², measured with horizontal measuring cups (following VW PV1210)

Copyright © 2026 by ASME; reuse license CC-BY 4.0

Downloaded from asmedigitalcollection.asme.org/OMAE/proceedings-pdf/OMAE2026/89480/V02AT02A050/7643410/v02at02a050-omae2026-177755.pdf by Deutsches Zentrum für Luft- und Raumfahrt (DLR) user on 22 October 2026

2. Truncate first and last 10% of each segment, to avoid transition effects from one climate phase into another.
3. Calculate statistical features for the truncated segments.
4. Depending on the duration, recalculate the features for several window sizes.
5. Evaluate the stability and compare features of the same baseline phases before and after the ageing cycle.

With the results for the different window sizes, the trend or stability of the considered features over the phase can be indicated. With the result for the whole truncated segment, a more averaged statement is made.

It should be considered that large window sizes lead to averaging but might hide interesting localized effects. Very small window sizes however are less suitable for a baseline comparison, since singularities, outliers or temporary external disturbances can gain influence on the result.

TABLE 4: STATISTICAL FEATURES (ABSTRACT)

Group	Feature
Location Measures	Mean
	Median
	Quartiles (25%, 75%)
Dispersion Measures	Standard deviation
	Peak to peak amplitude
	PSD total power
	PSD bandwidth
	SNR (linear or db)
Distribution Shape Measures	Skewness
	Kurtosis
	PSD flatness
Spectral Features	FFT dominant frequency
	PSD dominant frequency
	PSD spectral centroid
Stationarity Metrics	ADF statistic
	ADF p-value
Temporal Dependance	ACF for lag 1
	ACF lag at first 0
	ACF sum
Stability Metrics	ADEV min.
	ADEV tau at min.
	ADEV slope short-term
	ADEV slope long-term
Robustness Metrics	Number of missing values
	Number of outliers

It is a part of the research to determine which statistical features and which windowing are most suitable to detect ageing in this setup. Hence, we intend to derive more than 30 different statistical features from the time series. As outlined in table 4, they can be grouped into measures for location, dispersion, distribution, spectral features, stationarity, temporal dependance, stability and robustness of the acquired data. How the features relate to distinct characteristics or anomalies of the sensor data is exemplified in the following subsections.

5.1 Drift and long-term stability

Drift is the slow, systematic variation of the measurand. It can be characterized by a linear trend, a polynomial or other non-linear trends. We quantify drift using regression as well as stationarity- and stability-related features.

First of all, the Augmented Dickey-Fuller (ADF) test can be applied to evaluate if the time series is stationary [15]. A python implementation of the algorithm is available. It tests the null hypothesis that a unit root is present in a time series sample, which would mean the time series is non-stationary. The ADF result is given as its statistic and the p-value of its statistic. A value of $p < 0.05$ or a statistic value more negative than the critical value, reject the hypothesis and thus indicate the series is stationary. Vice versa, a high p indicates the series is non-stationary, which hints at a trend being present in the time series.

We estimate linear drift for each data segment, by fitting a linear trend line using least-squares regression:

$$y(t) = a + bt \tag{1}$$

where the slope b represents the linear drift rate. Furthermore, the coefficient of determination is calculated by:

$$R^2 = 1 - \frac{\sum_{i=1}^{n}(y_i - \hat{y}_i)^2}{\sum_{i=1}^{n}(y_i - \bar{y})^2} \tag{2}$$

where y_i are the values of the time series, $\hat{y}_i$ the associated regression values, $\bar{y}$ the mean of the series and n the number of data points. It is a common measure to quantify how much the regression line fits the actual time series. In addition, the residual variance is calculated by:

$$\hat{\sigma}_{res}^2 = \frac{1}{n-2}\sum_{i=1}^{n}(y_i - \hat{y}_i)^2 \tag{3}$$

It quantifies how much of the variation of the time series remains, after considering the linear trend. High residual variance may indicate a non-linearity like a seasonality or fluctuating noise in the data.

The auto-correlation function (ACF) is considered for further evaluation. It describes a time series by multiplication with a delayed version of itself, in order to find periodic dependencies. The autocorrelation at lag k is usually estimated by:

$$r_k = \frac{\frac{1}{N}\sum_{t=1}^{N-k}(z_t - \bar{z})(z_{t+k} - \bar{z})}{\frac{1}{N}\sum_{t=1}^{N}(z_t - \bar{z})^2} \tag{4}$$

where z_t is the time series, $\bar{z}$ is the mean value of the time series and N is the number of data points [16]. Several features can be derived from the ACF; at least the ACF for lag $k = 1$ and the ACF sum should be considered. If the function decays slowly, this creates high values for the ACF sum and hints at non-stationarity [17]. A wave-shaped non-linear trend would create

Downloaded from asmedigitalcollection.asme.org/OMAE/proceedings-pdf/OMAE2026/89480/V02AT02A050/7643410/v02at02a050-omae2026-177755.pdf by Deutsches Zentrum für Luft- und Raumfahrt (DLR) user on 22 October 2026

Copyright © 2026 by ASME; reuse license CC-BY 4.0

high values for lag k = 1 and the ACF plot also shows a wave-shape while it decays. Meanwhile, a non-deterministic trend like a random walk would yield $ACF \approx 1.0$ for lag $k = 1$ and the function would not decay at all.

Another powerful tool to evaluate the long-term stability of a time-series, which can be used as well to find a random walk, is the Allan variance. We use a Python implementation of its overlapped intervals form, which is defined as:

$$\sigma_y^2(\tau) = \frac{1}{2m^2(M-2m+1)} \sum_{j=1}^{N-2m} \left\{ \sum_{i=j}^{j+m-1} [y_{i+m} - y_i] \right\}^2 \quad (5)$$

where y_i is the ith of a set of M frequency values for averaging time $\tau = m \cdot \tau_0$, where m is the averaging factor and τ_0 is the basic measurement interval [16]. It is common to use its square root, the Allan deviation (ADEV). The ADEV provides magnitude versus time separation which in the form of a log–log deviation data plot allows the different noise and drift types to be identified by the slopes of the different plot regions [18]. Increased values at large τ for instance, together with a positive long-term slope, are characteristic for drift.

5.2 Noise and dispersion

Changes in sensor noise manifest as increased dispersion, altered distribution shape, higher temporal correlation or a shift of noise power across frequencies. Short-term variability is quantified through standard deviation and peak-to-peak amplitude. An increase in these metrics may indicate noise growth.

The power spectral density (PSD) characterizes how the signal power is distributed over frequencies. PSD-based features thus can be used to detect changes in spectral composition. In practice, the PSD is estimated from time-domain data using FFT-based methods with appropriate windowing. We use a Python-implementation of the method introduced by Welch, where:

$$\hat{P}(f_n) = \frac{L}{UK} \sum_{k=1}^{K} |A_k(n)|^2 \quad (6)$$

is the estimator of the power spectral density, for segments of length L, with number of segments K, while U is the window power term and $A_k(n)$ the Fourier-coefficients of the segment k at frequency index n [19].

Another possible measure to describe the advancement of noise in time-series data, is the signal-to-noise ratio (SNR). There are various definitions but in general it is the ratio of signal power to noise power:

$$SNR = \frac{P_{signal}}{P_{noise}} \quad (7)$$

Signal power is commonly estimated as the mean squared value of the signal, whereas noise power is obtained from the variance of the detrended residuals.

6. RESULTS AND DISCUSSION

To prove the concept that repeatable, stationary conditions can be created with the test stand and to characterize the stability of the considered statistical features for the unaged sensors, two test series at a temperature of 23 °C were recorded over 1 h, while the beam was at rest. A selection of results for one strain gauge[6], installed on top of the beam, is presented in the following figures. Both time series of the strain gauge are displayed in figures 4 and 5 as strain over time.[7] For graphical reasons, down-sampling was applied and a 0.1 Hz-version of the timeseries is displayed as the blue line, illustrating the character of the signal,

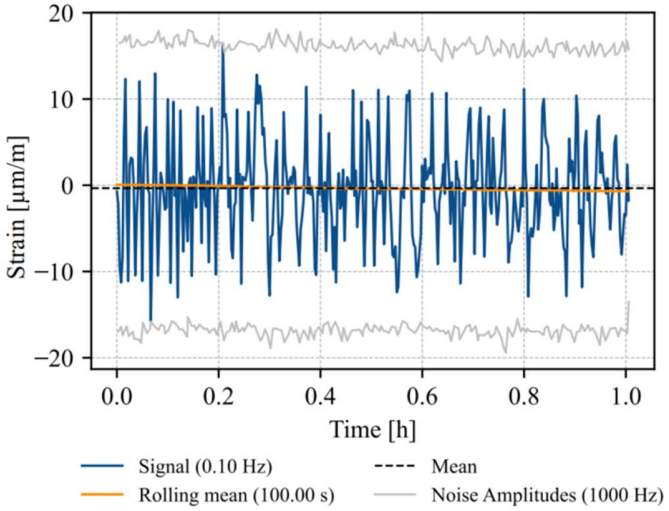


FIGURE 5: STRAIN GAUGE AT 23°C; SERIES 1

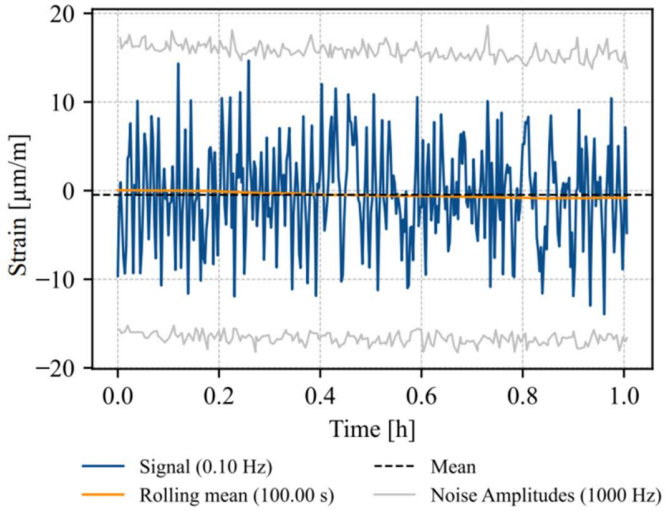


FIGURE 6: STRAIN GAUGE AT 23°C; SERIES 2

[6] Film-strain gauge (film: polyimide, grid: constantan) in quarter-bridge 4-wire circuit (cable resistance compensated) with 350 Ohm. Surface polished before application with strain gauge adhesive HBM CA80.

[7] The strain was internally calculated in the data acquisition software with the gauge factor according to the strain gauge calibration certificate.

Downloaded from asmedigitalcollection.asme.org/OMAE/proceedings-pdf/OMAE2026/89480/V02AT02A050/7643410/v02at02a050-omae2026-177755.pdf by Deutsches Zentrum für Luft- und Raumfahrt (DLR) user on 22 October 2026

Copyright © 2026 by ASME; reuse license CC-BY 4.0

while the grey lines indicate the noise amplitudes of the original signal, which was digitized with 1000 Hz. The mean of the whole segment is displayed as a dotted black line, while a rolling mean with a window size of 100 s is indicated as an orange line.

First of all, it becomes clear both time series are generally stable, without any unexpected shifts and constant noise levels. The dispersion measures (see table 5) present only slight differences between the two series, indicating comparable short-term noise characteristics. Furthermore, both time series have a minor mean offset from zero. On closer inspection of the orange rolling mean line, both time series show a minor decreasing trend. This is likewise quantified by the slopes of the fitted linear trends (see table 5). Both series have a slight negative trend, while in series 2 the slope has decreased by 34% and the determination has increased by 92%. This indicates that the trend characteristics between series 1 and 2 are different and series 2 has a stronger trend which is closer to a linear trend. After this rough overview, the following figures reveal more details.

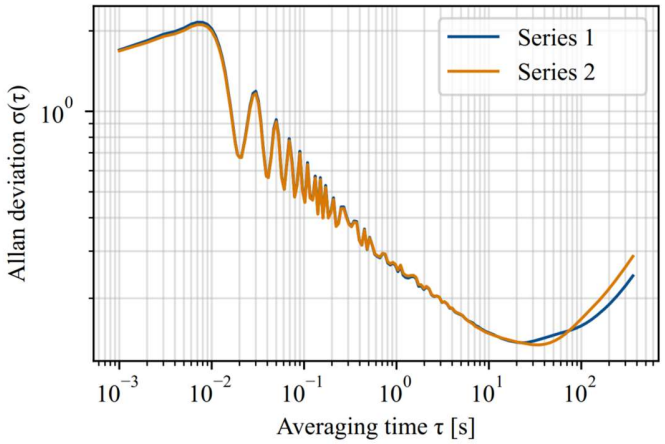


FIGURE 7: STRAIN GAUGE AT 23°C; ADEV LOG-LOG-PLOT SERIES 1 AND 2

The ADEV log-log-plot for both time series is displayed in Figure 7. As mentioned in section 5.1, the interpretation of these plots considers the slopes of different plot regions [18]. In the short-term region between $\tau = 10^{-3} \dots 10^{-2}$ both series almost coincide with a slope of about 0.19. This indicates a deviation from ideal white noise, which would produce a short-term slope of -0.5 in theory. However, it can be stated that the high-frequency noise characteristic does not change between the two series. In the middle part of the plot, again the two series almost perfectly coincide. Interestingly it shows a continues slope with a wave like deviation which hints at a very regular frequency component in the data. The peaks of the deviations in the middle part pose regular distances of 0.02 s which hint towards a 50 Hz frequency component in the data. This will be addressed again further below in the discussion of the PSD. The long-term area on the right side of the plot presents a higher deviation between the two lines. Both series show a significant positive slope in this region, which confirms a trend being present in both data sets. The minimum ADEV of series 1 comes in earlier and the line after that shows a rather non-linear increase. The minimum ADEV of series 2 comes in 67% later and the line after that shows an almost linear increase. Together with the significantly higher coefficient of determination for series 2, which was mentioned earlier, this suggests series 1 indeed has a considerable non-linear component in its trend. An analysis of the temperature trends from a temperature sensor on the beam surface revealed, this deviation might be caused by the temperature control curve. Although the temperature only presented slight deviations of $\pm 0{,}5°C$ over both series, the temperature trend in the first series has stronger fluctuations while the temperature trend of series 2 is comparably smooth. The strain gauges are temperature-compensated for steel but a certain degree of temperature sensitivity typically remains.

The results for the ACF are not discussed in detail, but the selection of ACF features in table 5 confirms a very similar short-term behavior and a stronger trend in series 2 once again.

TABLE 5: ABSTRACT AND COMPARISON OF STATISTICAL FEATURES FOR STRAIN GAUGE SERIES 1 AND 2

Feature	Series 1	Series 2	Dev.
Location			
Mean	-0.341	-0.475	39 %
Median	-0.347	-0.480	38 %
Q1 (25%)	-3.29	-3.36	2.1 %
Q3 (75 %)	2.62	2.42	-7.6 %
Dispersion			
Standard deviation	5.47	5.28	-3.5 %
P2P amplitude	37.6	36.9	-1.8 %
PSD power	29.8	27.7	-6.9 %
PSD bandwidth	98.6	101	2.4 %
SNR (linear)	1.00	1.01	0.4 %
Spectral			
PSD dominant freq.	50.8	50.8	0.0 %
PSD spectral centr.	102	104	2.3 %
Temporal			
Linear trend slope	-2.15E-07	-2.88E-07	34 %
Determination	1.69E-03	3.24E-03	92 %
Residual variance	29.8	27.8	-6.9 %
ACF for lag 1	0.723	0.712	-1.5 %
ACF lag first 0	6	6	0.0 %
ACF sum	289	577	100 %
Stability			
ADEV min	0.0182	0.0167	-8.3 %
ADEV tau at min	24.3	40.7	67 %
ADEV slope short	0.197	0.187	-5.3 %
ADEV slope long	0.135	0.346	157 %

As a last result, the PSD-plot is shown in figure 8. The graphs of series 1 and 2 almost perfectly coincide. They consist of a horizonal line over the whole frequency spectrum, with some equally spaced peaks. The horizontal line represents a DC-

Downloaded from asmedigitalcollection.asme.org/OMAE/proceedings-pdf/OMAE2026/89480/V02AT02A050/7643410/v02at02a050-omae2026-177755.pdf by Deutsches Zentrum für Luft- und Raumfahrt (DLR) user on 22 October 2026

Copyright © 2026 by ASME; reuse license CC-BY 4.0

component in the signal, which is expected from the measurement of a static strain. The highest peak in the PSD-plot occurs at a frequency of 50 Hz. In accordance with the deviations in the central part of the ADEV log-log-plot, further peaks appear at multiples of that value. Apart from that, no other dominant frequencies are detectable. The latter coincides with the power grid frequency in Germany. It is suspected that the peaks are indeed power-line interferences in the DC supply voltage, coming from the measuring device. Power line interference is a known phenomenon but it illustrates the analytic insight achievable with the presented statistical method pretty well.

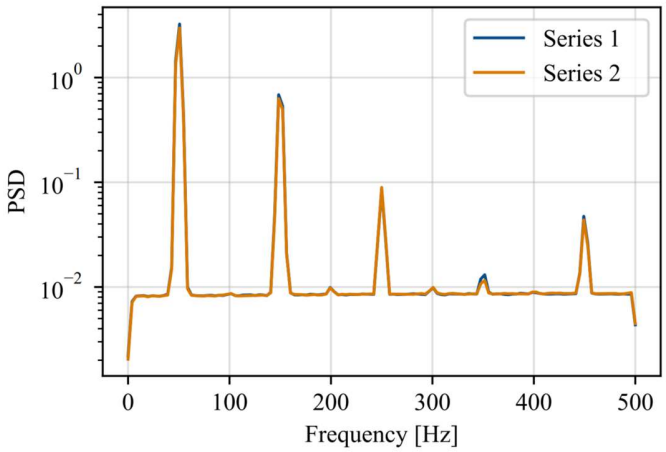


FIGURE 8: STRAIN GAUGE AT 23°C; PSD-PLOT SERIES 1, 2

We summarize, the agreement of the two series regarding their location, dispersion and spectral composition is good. No unexpected shifts or spikes have occurred in the data. Meanwhile, there is a difference in the drift shape and drift intensity between the two series, which was not anticipated. The results highlight the need for thorough baseline characterization prior to commencing the ageing experiments. The temperature control behavior of the chamber has to be studied in the long-term. Longer warmup periods prior to tests might be needed. Also, it has to be considered that the beam is in contact with the ambience outside the chamber (see figure 1) and its equilibrium temperature is thus influenced by the surrounding as well. Apart from that, other yet undetected disturbances can not be ruled out either.

7. CONCLUSION

A test stand featuring a corrosion test chamber and a beam structure has been constructed and commissioned. A test program, data analysis approach and essential statistical features were outlined. A test series of a strain gauge in a stationary climate has been recorded and analyzed.

8. OUTLOOK

It is planned to extend the test stand features and improve its control quality. This is meant to rectify the present challenges with the trend stability. Furthermore, we want to enable certification tests according to prevailing standards with the test stand in the future. In the maritime sector, classification societies provide the needed guidelines, to test and approve equipment for application in practice. As an example, the DNV class guideline DNV-CG-0339 will be briefly outlined here. It constitutes the "Environmental test specification for electrical, electronic and programmable equipment and systems" and is thereby in the scope of rules for classification of control and monitoring systems [11]. The described procedures for the equipment under test (EUT) are generally tied to the intended main area on board of a ship, like machinery spaces, control rooms or open deck and distinguishes between different location classes within these main areas, like inside consoles, on machinery or in submerged condition. The tests include dry heat, cold, damp heat, vibration and others. In order to fulfill the test requirements for the minimum location class A, a test stand would need to feature temperature ranges from $+5\,°C$ to $+55\,°C$ with an accuracy of $\pm 2\,°C$, relative humidity of up to $95\,\%$ with a tolerance of $\pm 10\,\%$ and continuously controllable sweep sine vibration from $2 \ldots 100$ Hz with an accuracy of $\pm 10\,\%$. Regarding the ambient control sensors, the humidity sensor in the test setup needs to be circulated by a continuous air flow of $1{,}5 \ldots 2{,}0 m/s$ and the temperature sensors must not be in the sphere of influence of possible waste heat from the EUT. For the mechanical tests, the EUT has to be vibrated in three mutually perpendicular planes and has to be installed in orientation as in normal service. Tests are supposed to be carried out by accredited laboratories or comparable facilities. This list of requirements elucidates typical prerequisites for a test stand, to conduct certification tests for electronic equipment in maritime applications.

It is planned to proceed with a collection and analysis of further rules and relevant norms to expand the test stand functions accordingly, enabling to serve diverse scientific and industrial demands in the future.

REFERENCES

[1] Silva-Campillo, Arturo; Pérez-Arribas, Francisco; Suárez-Bermejo, Juan Carlos (2023): Health-Monitoring Systems for Marine Structures: A Review. In: *Sensors (Basel, Switzerland)* 23 (4). DOI: 10.3390/s23042099.

[2] Kahl, Adrian; Fricke, Wolfgang; Paetzold, Hans; Selle, Hubertus von (2015): Whipping Investigations Based on Large-Scale Measurements and Experimental Fatigue Testing. In: *IJOPE* 25 (4). DOI: 10.17736/ijope.2015.sh14.

[3] Böhm, Angelo Mario; Bock und Polach, Rüdiger Ulrich Franz von; Herrnring, Hauke; Ehlers, Sören (2021): The measurement accuracy of instrumented ship structures under local ice loads using strain gauges. In: *Marine Structures* 76, S. 102919. DOI: 10.1016/j.marstruc.2020.102919.

[4] Waal, Rosca J.O. de; Bekker, Anriëtte; Heyns, P. Stephan (2017): Bi-Polar Full-Scale Measurements of Operational Loading on Polar Vessel Shaft-Lines. In: *Proceedings of the 24th International Conference on Port and Ocean Engineering under Arctic Conditions, POAC'17, Busan, Korea* June 11-16.

Downloaded from asmedigitalcollection.asme.org/OMAE/proceedings-pdf/OMAE2026/89480/V02AT02A050/7643410/v02at02a050-omae2026-177755.pdf by Deutsches Zentrum für Luft- und Raumfahrt (DLR) user on 22 October 2026

Copyright © 2026 by ASME; reuse license CC-BY 4.0

[5] Yang, Sujun; Shi, Lei; Chen, Demin; Dong, Yuqing; Hu, Zhenyi (2017): Development of ship structure health monitoring system based on IOT technology. In: *IOP Conf. Ser.: Earth Environ. Sci.* 69, S. 12178. DOI: 10.1088/1755-1315/69/1/012178.

[6] Andoniu, A.; Lauzon, J. de; Lamaison, V. (2019): Full scale measurements of the hydro-elastic behavior of a 13000 TEUs container ship. In: J. Parunov und C. Guedes Soares (Hg.): Trends in the Analysis and Design of Marine Structures: CRC Press, S. 319–328.

[7] Hassan, Ietezaz Ul; Panduru, Krishna; Walsh, Joseph (2024): An In-Depth Study of Vibration Sensors for Condition Monitoring. In: *Sensors (Basel, Switzerland)* 24 (3). DOI: 10.3390/s24030740.

[8] Wei, Pengyu; Li, Chuntong; Jiang, Ze; Wang, Deyu (2024): Real-Time Digital Twin of Ship Structure Deformation Field Based on the Inverse Finite Element Method. In: *JMSE* 12 (2), S. 257. DOI: 10.3390/jmse12020257.

[9] Krishnamurthi, Rajalakshmi; Kumar, Adarsh; Gopinathan, Dhanalekshmi; Nayyar, Anand; Qureshi, Basit (2020): An Overview of IoT Sensor Data Processing, Fusion, and Analysis Techniques. In: *Sensors (Basel, Switzerland)* 20 (21). DOI: 10.3390/s20216076.

[10] Bartels, Jan-Hauke; Marx, Steffen (2025): Addressing Time Variance in Measurement Systems with Bayesian Model Updating. In: *Sensors and Materials* 37 (3), S. 921. DOI: 10.18494/SAM5393.

[11] Class Guideline DNV-CG-0339, August 2021: Environmental test specification for electrical, electronic and programmable equipment and systems.

[12] dos Reis, João; Oliveira Costa, Carlos; Da Sá Costa, José (2018): Strain gauges debonding fault detection for structural health monitoring. In: *Struct Control Health Monit* 25 (12), e2264. DOI: 10.1002/stc.2264.

[13] Khaled, K. M.; Mahmoud, G. M. (2018): An investigation on the effect of humidity on the zero signal of a strain gauge measuring system. In: *Univ. Sci.* 23 (1), S. 129. DOI: 10.11144/Javeriana.SC23-1.aint.

[14] Bartels, Jan-Hauke; Potthast, Thomas; Möller, Sören; Grießmann, Tanja; Rolfes, Raimund; Beer, Michael; Marx, Steffen (2024): Robust SHM: Redundancy approach with different sensor integration levels for long life monitoring systems. In: *eJNDT* 29 (7). DOI: 10.58286/29699.

[15] Dickey, David A.; Fuller, Wayne A. (1979): Distribution of the Estimators for Autoregressive Time Series With a Unit Root. In: *Journal of the American Statistical Association* 74 (366), S. 427. DOI: 10.2307/2286348.

[16] Riley, W. and Howe, D. (2008), Handbook of Frequency Stability Analysis, Special Publication (NIST SP), National Institute of Standards and Technology, Gaithersburg, MD, [online], *https://tsapps.nist.gov/publication/get_pdf.cfm?pub_id=50505* (Accessed December 7, 2025)

[17] Box, George (2013): Box and Jenkins: Time Series Analysis, Forecasting and Control. In: Terence C. Mills (Hg.): A Very British Affair. London: Palgrave Macmillan UK, S. 161–215.

[18] Land, D. V.; Levick, A. P.; Hand, J. W. (2007): The use of the Allan deviation for the measurement of the noise and drift performance of microwave radiometers. In: *Meas. Sci. Technol.* 18 (7), S. 1917–1928. DOI: 10.1088/0957-0233/18/7/018.

[19] Welch, P. (1967): The use of fast Fourier transform for the estimation of power spectra: A method based on time averaging over short, modified periodograms. In: *IEEE Trans. Audio Electroacoust.* 15 (2), S. 70–73. DOI: 10.1109/TAU.1967.1161901.

Downloaded from asmedigitalcollection.asme.org/OMAE/proceedings-pdf/OMAE2026/89480/V02AT02A050/7643410/v02at02a050-omae2026-177755.pdf by Deutsches Zentrum für Luft- und Raumfahrt (DLR) user on 22 October 2026

Copyright © 2026 by ASME; reuse license CC-BY 4.0